α-$CrCl_2$ under Pressure: Prediction of a Metallic Phase Transition†

Andreas Hermann* and Peter Schwerdtfeger*

Centre for Theoretical Chemistry and Physics (CTCP), New Zealand Institute for Advanced Study (NZIAS), Massey University Albany, Private Bag 102904, North Shore MSC, Auckland, New Zealand

Received: May 9, 2009; Revised Manuscript Received: June 17, 2009

The volume−pressure behavior for the α-$CrCl_2$ phase is studied at the density functional level of theory. The calculations predict a metallic phase transition at 15 GPa from a generalized gradient approximation. The addition of an on-site Hubbard repulsion term shifts this transition to 35 GPa. Higher pressure leads to significant changes in the octahedral ligand environment around the Cr atoms, changing from a prolate to oblate environment toward the metallic phase, and the local magnetic moments collapse close to the metallic phase transition.

Introduction

The application of high pressure to solid materials has recently become an intense research field,[1,2] because new materials can be stabilized, often unusual structure are formed,[3,4] and new physicochemical properties can arise.[5−7] On the experimental side, great progress has been made to achieve high pressures up to about 500 GPa.[8] However, even for the simplest interacting systems, it is currently not straightforward to obtain accurate isotherms (volume−pressure curves) up to high pressures and interpret the observed phase transitions. On the theoretical side, highly accurate wave function based methods such as coupled-cluster theory are currently limited to small- to medium-sized molecules, although such methods have been used more recently to model the pressure-induced dimerization of dimethylacetylene.[9] Wave-function-based methods soon become computationally intractable for larger systems and, for the solid state, are currently applicable only for systems with a sizable band gap (i.e., insulators), although some progress has been made very recently in describing metallic systems.[10−13] It is therefore no surprise that the main workhorse in high-pressure simulations of solid-state materials is density functional theory (DFT).

There are, however, a number of well-known difficulties associated with the application of density functional theory, such as the generalized gradient approximation (GGA) for the solid state. For example, van der Waals-type correction terms[14] are required to accurately describe molecular crystals. Conroy et al. showed, for example, that for the isotherms of nitromethane, the inclusion of an empirical van der Waals term considerably improves the agreement with experiment.[15] Moreover, strongly correlated systems, such as Mott insulators in transition metal and f-element compounds, are not well described by the GGA,[16] and one usually resolves this situation by adding a Hubbard on-site repulsion term (DFT + U) to correctly describe many-body effects.[17] Prime examples here are MnO, FeO, and hematite,[16,18,19] all of which have been studied under pressure using the GGA + U approach,[20] or the δ-phase of plutonium.[21] Here, we should also mention recent progress in designing new functionals for the solid state, such as the screened hybrid functional, which seem to be capable of correctly describing strongly correlated systems.[22]

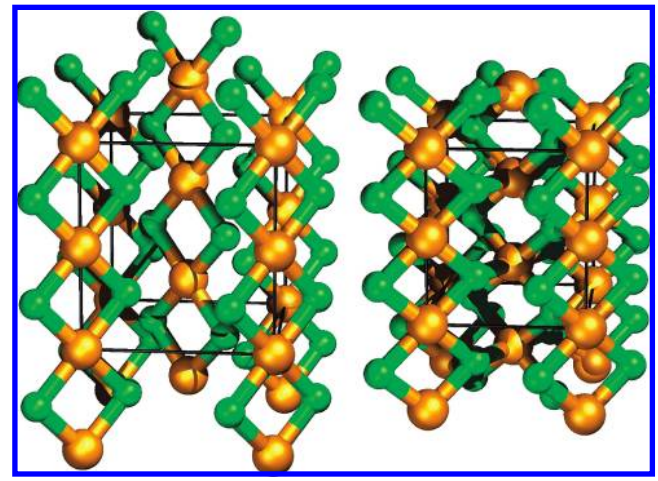

Figure 1. Crystal structure of α-$CrCl_2$. Left: relaxed ground state; right: under pressure, $p \approx 400$ kBar. Golden (green) spheres denote Cr (Cl) atoms. Magnetic unit cell of antiferromagnetic ground state is indicated.

In our recent work on the magnetic ground state of α-$CrCl_2$,[23] we showed that the GGA + U approach leads to spin-coupling constants that, in contrast to the GGA, are in good agreement with experimental data.[24] Hence, this approach should be ideal for correctly describing the ferro-/antiferromagnetic phases of α-$CrCl_2$ at higher pressures. Figure 1 depicts the rather intriguing crystal structure of α-$CrCl_2$. It has a simple orthorhombic unit cell (space group P_{nnm}) in which each Cr atom is surrounded by a distorted octahedron of Cl atoms. The primitive unit cell contains two $CrCl_2$ units that form chains along the crystallographic *c* axis: adjacent Cr atoms form four-membered Cr_2Cl_2 rings along the *c* axis that are doubly bridged by Cr−Cl−Cr bonds. Studying the $CrCl_2$ molecule even in the gas phase is a challenge for experimentalists and theoreticians alike:[25] the question whether the $CrCl_2$ molecule is linear or bent due to a Jahn−Teller distortion was vividly discussed among different groups.[26−32] On the experimental side, electron-diffraction structural analysis is hindered by spontaneous formation of $(CrCl_2)_n$ clusters up to $n = 4$ in the gas phase, and exact theoretical calculations need to take into account the multireference character of the electronic ground state.[25] However, it can be concluded that in the earliest stages of $CrCl_2$ nucleation,

† Part of the "Walter Thiel Festschrift".

* E-mail: a.h.hermann@massey.ac.nz; p.a.schwerdtfeger@massey.ac.nz.

10.1021/jp904325v CCC: $40.75
Published on Web 07/16/2009

small clusters up to the tetramer $(CrCl_2)_4$ form in a chainlike structure surprisingly similar to the structural motif found in the solid state. A similar situation is found for CrF_2.[33]

The magnetic moments localized at the Cr atoms are found to prefer an antiferromagnetic coupling between adjacent Cr centers, albeit with only small energy differences between different magnetic schemes.[23] For the crystalline phase, several different macroscopic magnetic coupling schemes are conceivable: a ferromagnetic (FM), antiferromagnetic (AFM), or nonmagnetic structure. The latter could not be stabilized in any of our previous calculations.[23] For an antiferromagnetic crystal, one can construct ferromagnetic $CrCl_2$ chains (with opposite spin alignment for adjacent chains, here denoted AFM/FM), or antiferromagnetic chains (with alternating spin alignment for Cr atoms *within* the chains, here denoted AFM/AFM). In our previous work, we established that in the ground state, α-$CrCl_2$ is coupled antiferromagnetically along the *c* axis chains, thus favoring the AFM/AFM state, in agreement with gas phase cluster calculations.[25] Like in transition metal oxides, we expect a metallic phase transition at higher pressures. However, it is currently not known from experiment at what pressure this transition occurs. We therefore present a computational study using the GGA + U approach for the pressure dependence (isotherm at 0 K) of the α-$CrCl_2$ phase and predict a metallic phase transition at pressures of around 35 GPa.

Computational Method

The crystalline properties of α-$CrCl_2$ are calculated using DFT in conjunction with a plane wave basis set, as implemented in the Vienna Ab-initio Simulation Package.[34] The electron−electron interaction is modeled using the generalized gradient approximation[35] of the exchange-correlation energy by Perdew and Wang (PW91). As mentioned before, in strongly correlated systems, such as for localized transition metal d orbitals, the on-site Coulomb repulsion is, in general, not well described by the GGA. We thus use the GGA + U approach,[17,36−38] in which a penalty function is added to the GGA (here, PW91) total energy expression, that drives the on-site density matrix ρ_{ij}^{σ} toward idempotency:

$$E_{\mathrm{GGA+U}} = E_{\mathrm{GGA}} + \frac{U-J}{2}\sum_{\sigma}\mathrm{Tr}[\rho^{\sigma} - \rho^{\sigma}\rho^{\sigma}] \qquad (1)$$

The parameters *U* and *J* describe the energy required to add an additional d electron to the atomic site and the screened exchange energy, respectively. In the present implementation, only their difference, $U - J$, contributes to the total energy. In our previous work, we found a very good agreement with experimentally derived magnetic coupling constants in the optimized ground state for $U - J = 1.8$ eV[23] in the GGA + U approach, realized through $U = 2.8$ eV and $J = 1.0$ eV. Unless mentioned otherwise, the same value for $U - J$ is used here. The electron−ion interaction is modeled within the frozen-core approximation, realized in the framework of the projector augmented wave method (PAW).[39,40] The PAW method allows for access to the all-electron wave functions on the atomic sites, but also allows restriction of the plane wave expansion of the electronic orbitals to a rather moderate cutoff of 450 eV in the present case. A total of six electrons for each Cr atom ($3d^5 4s^1$) and seven electrons for each Cl atom ($3s^2 3p^5$) are included in the valence space. Reciprocal space integrations are carried out on a regular mesh in reciprocal space, equivalent to 128 k-points in the Brillouin zone of the primitive α-$CrCl_2$ unit cell. We consider a structure to be in equilibrium if each Cartesian component of the atomic forces is less than 5 meV/Å. We fit the resulting $E(V)$ curve with a Vinet equation of state (EOS).[41] Note that this needs refined lattice constants, as compared to our previous study.[23]

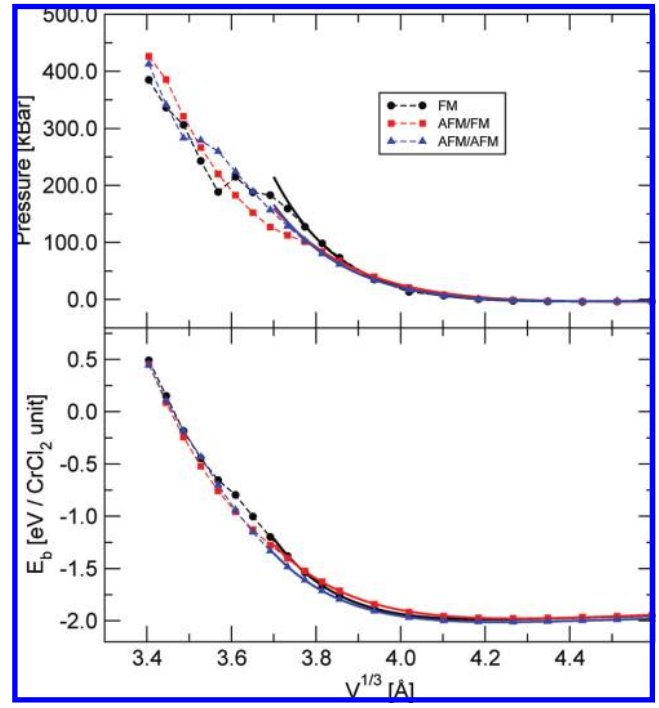

Figure 2. Total energies (lower panel) and pressures (upper panel) against volume, *V*, per molecular $CrCl_2$ unit. Circles (squares, triangles) denote FM (AFM/FM, AFM/AFM) spin coupling. See text for details. Solid lines show $E(V)$ and $p(V)$ fits near the global minima. For the orthorhombic lattice, the volume is given by $V = abc$ with *a*, *b*, and *c* being the lattice constants given in Table 1.

Results and Discussion

In Figure 2, total energies and corresponding pressures from GGA calculations are plotted against the "effective lattice constant" $V^{1/3}$ (*V* being the volume of the system) for the three magnetic structures: the ferromagnetic structure, and two antiferromagnetic structures with ferro- and antiferromagnetic intrachain coupling.[23] Ground state properties derived near the global minima are compiled in Table 1. Binding energies of the solid state are given per $CrCl_2$ unit, with respect to the gas phase energy of a $CrCl_2$ molecule (calculated in a large super cell using the same methods and numerical parameters). The AFM/AFM structure is the energetic ground state[23] in good agreement with X-ray diffraction measurements.[42] The spin separation energies are, however, quite small: about 30 meV per $CrCl_2$ unit favoring the AFM/AFM coupling over FM and AFM/FM. The lattice constants of the calculated ground state are within about 6% (for *a* and *b* lattice constants) and 2.5% of the experimental values (for *c* lattice constant). Accordingly, the intrachain Cr−Cl distance d_1 is very close to experiment, but the interchain distance d_2 is somewhat too large, thus indicating that the Cr−Cl−Cr bridging bonds within the $CrCl_2$ chains are well-described, whereas the interchain interaction is not fully accounted for, possibly due to the incorrect long-range behavior of the GGA functional used. The parameter B_0 (bulk modulus) and its pressure derivative B' required for the Vinet EOS are also given in Table 1. Not surprisingly, the $E(V)$ data—or better, the $p(V)$ data—show that the rather simple

TABLE 1: Ground State Properties of α-$CrCl_2$, from DFT-GGA and GGA + U calculations[a]

method	State	E_b	B_0	B'	a_0	b_0	c_0	x	y	d_1	d_2
exp[42]					6.65	5.99	3.49	0.362	0.274	2.40	2.91
GGA	FM	−2.02	54.4	12.7	6.74	6.33	3.48	0.348	0.302	2.38	3.02
	AFM/FM	−2.01	50.8	9.8	7.00	6.28	3.45	0.371	0.286	2.37	3.16
	AFM/AFM	−2.04	47.6	11.2	6.91	6.33	3.41	0.357	0.293	2.36	3.09
GGA + U											
$U = 1.0$ eV	AFM/AFM	−2.04	47.6	11.2	6.91	6.33	3.41	0.357	0.293	2.36	3.09
$U = 2.0$ eV	AFM/AFM	−2.16	63.7	9.4	6.95	6.36	3.44	0.359	0.293	2.38	3.11
$U = 2.8$ eV	FM	−2.24	70.2	9.3	6.88	6.34	3.51	0.357	0.294	2.40	3.08
$U = 2.8$ eV	AFM/FM	−2.24	72.4	9.1	7.00	6.29	3.49	0.369	0.285	2.39	3.14
$U = 2.8$ eV	AFM/AFM	−2.25	72.6	9.2	6.95	6.35	3.47	0.359	0.292	2.39	3.11
$U = 4.0$ eV	AFM/AFM	−2.41	84.4	8.9	6.90	6.31	3.51	0.358	0.289	2.41	3.07
$U = 5.0$ eV	AFM/AFM	−2.54	95.4	8.6	6.85	6.29	3.54	0.356	0.287	2.43	3.04

[a] Binding energies E_b per $CrCl_2$ unit (in eV); bulk moduli B_0 (in kbar) and its pressure derivative B'; lattice constants a_0, b_0, c_0; Wyckoff positions x, y of Cl atoms, intra- (d_1) and interchain (d_2) Cr−Cl distances (Ångstroms). For the GGA + U calculations, $J = 1.0$ eV was used.

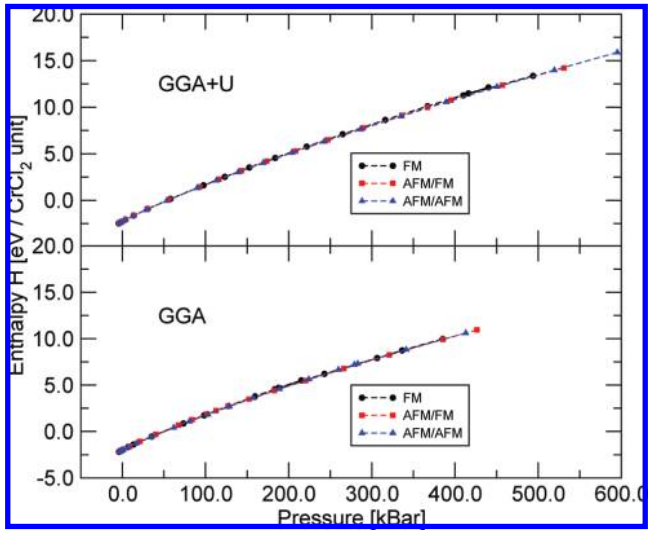

Figure 3. Enthalpies of different magnetic phases (see text) from GGA (lower panel) and GGA + U calculations (upper panel).

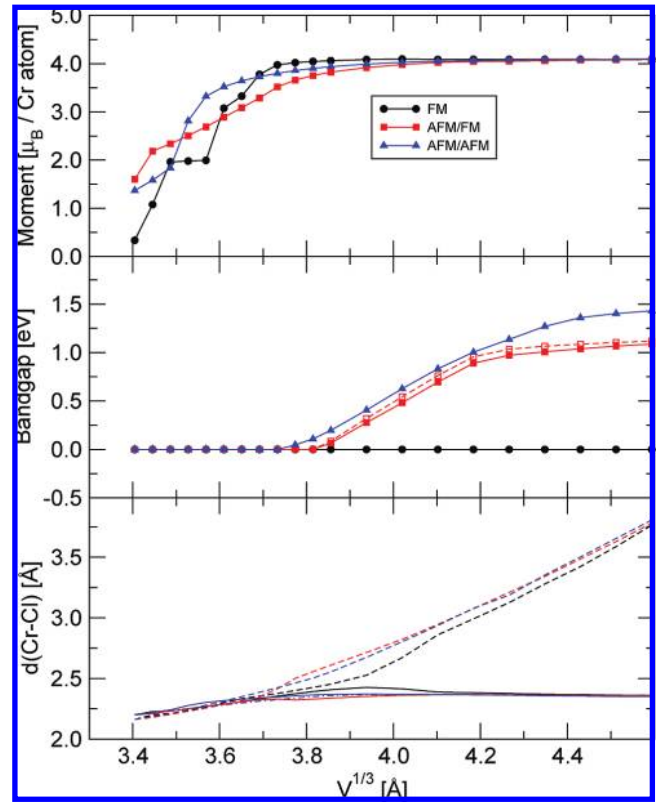

Figure 4. From top: magnetic moments, band gaps, and internal Cr−Cl bond lengths, depending on lattice constant, and for various magnetic coupling schemes. Bond lengths: solid (dashed) lines for intra- (inter-) chain distances.

classical approach for the Vinet EOS (namely, a linear dependence of the bulk modulus B on the pressure) holds only for low pressures up to about 130 kBar. For higher pressures, all $E(V)$ and $p(V)$ curves deviate significantly from the EOS fit around the minimum. At high pressures, all three magnetic phases are predicted to undergo a phase transition, clearly visible as kinks in the $p(V)$ curves in Figure 2. Up to very high pressures of 400 kBar (or 40 GPa), only small energy differences separate the three magnetic phases. For better comparison of the different phases, the respective enthalpies $H = E + pV$ are shown in Figure 3 (which also shows results from GGA + U calculations; see below). The energy differences in the enthalpies are very small, thus preventing an unambiguous assignment of the favored magnetic order under finite pressure.

The structural, electronic, and magnetic properties in α-$CrCl_2$ are closely connected (see Figure 4). There, the intra- and interchain Cr−Cl bond lengths d_1 and d_2 as well as the electronic band gap and the magnetic moments of the Cr atoms are plotted versus the lattice constant. At large lattice constants (negative pressure), the $CrCl_2$ chains remain structurally stable: the intrachain Cr−Cl distance is constant (even decreasing with increased lattice constant), whereas the interchain Cr−Cl distance increases linearly with increased lattice constants. Thus, under negative pressure, $CrCl_2$ decomposes into an assembly of disconnected $CrCl_2$ chains. This explains the unusual flat potential energy surface of $CrCl_2$ at large unit cell volumes. Both electronic band gap and magnetic moments are basically constant in this regime. Under increased pressure, however, the interchain distance decreases, effectively changing the ligand environment of the Cr atoms from a prolate to an oblate octahedron at high pressures. It also leads to a closing of the electronic band gap. For lattice constants below 3.75 Å, at pressures of more than about 150 kBar, all magnetic structures are metallic. Although DFT-GGA is known to underestimate the electronic band gap, due to a nondiscontinuity of the exchange-correlation potential,[43] it should describe the trend of the decreasing and eventually vanishing band gap correctly. The metallic phase transition is accompanied by a collapse of the local magnetic moments (see upper panel of Figure 4). Although the magnetic order is still existent even at the highest investigated pressures of around 400 kBar, the local spin quantum numbers are significantly lower than the low pressure value of $S = 2$.

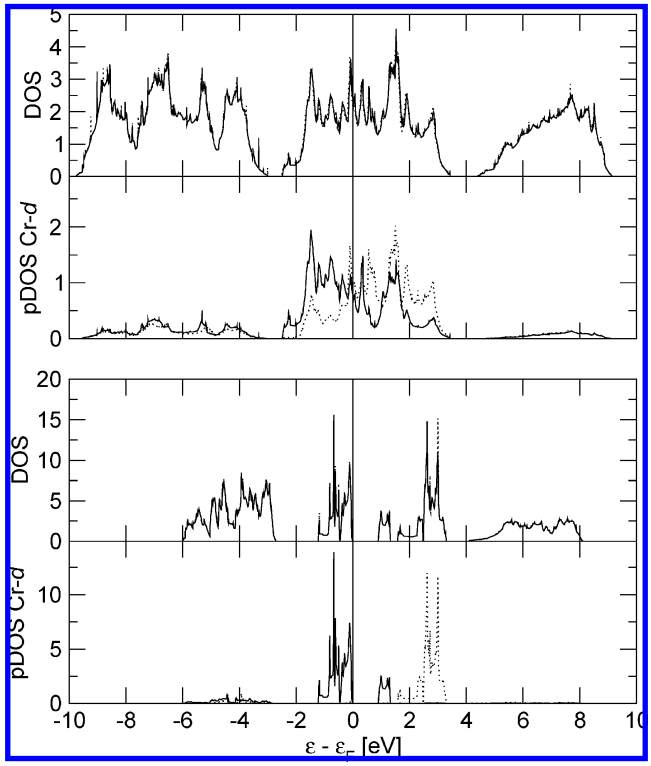

Figure 5. Electronic density of states of AFM/FM structure, from GGA calculations. Upper panel, pressure $p \approx 400$ kBar; lower panel, $p = 0$. Total DOS and Cr site-projected partial DOS of d electrons are shown, respectively. Solid (dotted) lines denote $m_z = +1$ (-1) spin quantum number. Energies are normalized to the Fermi level, ε_F.

The changes of the electronic properties under pressure can also be visualized in the electronic density of states (DOS) (see Figure 5). In the optimized ground state, the Cr-centered 3d bands are split, with an electronic band gap of about 0.8 eV. Both valence and conduction band edges are of 3d character. The d bands are well-separated from the Cl 2p states which are $-3\cdots -6$ eV below the Fermi level. The different spin directions of the 3d electrons are separated by about 3 eV, leading to the local magnetic moment of about 4 μ_B in the ground state. Under pressure, however, increased electronic dispersion and interaction between the spin centers lead to a metallic electronic state (see upper panel of Figure 5). The splitting of the different spin levels is lifted, which leads to the collapse of the local magnetic moments, as mentioned above. The Cr 3d states also mix increasingly with the Cl 2p electrons. In Figure 6, the band structure of the 3d electrons of the AFM/FM phase is displayed close to the onset of metallicity. Analyzing the band structures, we see that the population of the lowest conduction band occurs first between the special points S (110) and R (111) in the Brillouin zone. That corresponds to the body diagonal connecting adjacent chains. At much higher pressure, intrachain metallic character appears.

In Figure 7, total energies and pressures from GGA + U calculations are plotted for the magnetic coupling schemes discussed above. As in GGA, the ground state is found to be the AFM/AFM configuration. Table 1 lists in detail structural properties of the global minima of the various magnetic schemes; they agree well with experimental data. The largest error is made by an underestimated coupling between the $CrCl_2$ chains, leading to lattice constants a and b that are too large. In addition, the interchain Cr−Cl distance is too large when compared to experiment. Again, the energy differences between the different magnetic states are found to be very small, on the

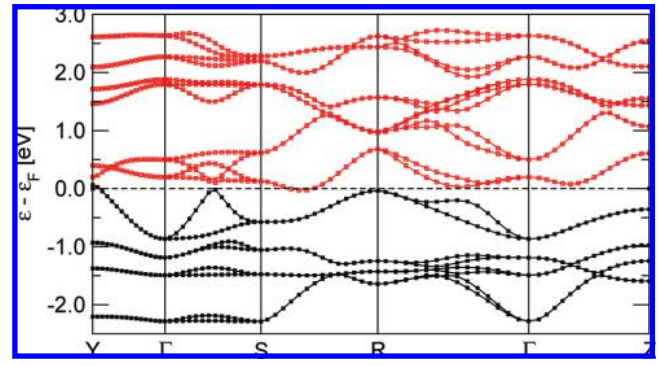

Figure 6. Electronic band structure of AFM/FM structure. From GGA calculations, at pressure $p \approx 100$ kBar. Black (red) squares indicate valence (conduction) bands. Energies normalized to Fermi energy ε_F (dashed line).

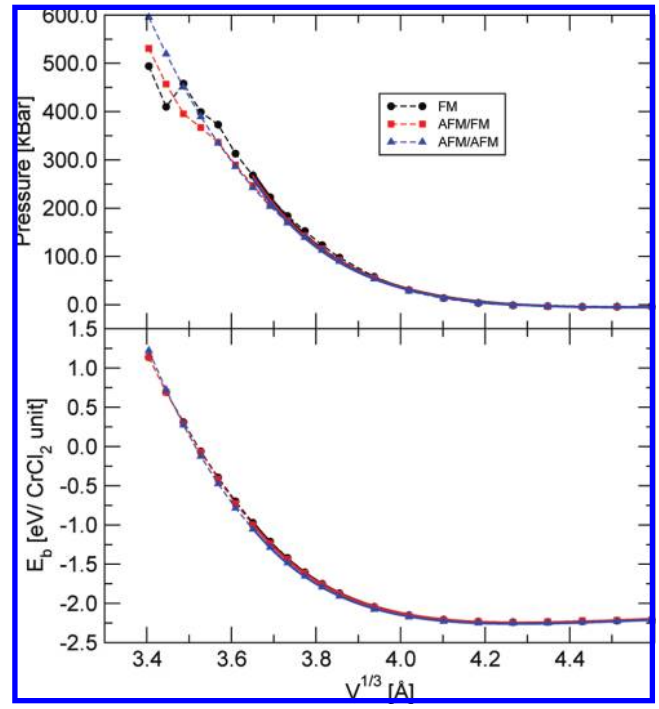

Figure 7. Total energies (lower panel) and pressures (upper panel) against volume, V, per molecular $CrCl_2$ unit, from GGA + U calculations ($U - J = 1.8$ eV). Circles (squares, triangles) denote FM (AFM/FM, AFM/AFM) spin coupling (see text for details). Solid lines show $E(V)$ and $p(V)$ fits near the global minima.

order of 10 meV per $CrCl_2$ unit. As shown in Figure 7, these energy differences are even smaller under high pressure. In addition, a phase transition occurs around 350 kBar or 35 GPa, visible in the $p(V)$ curves in Figure 7. This phase transition is accompanied by qualitative changes in the magnetic and electronic properties (see Figure 8) as $CrCl_2$ becomes metallic, and the local magnetic moments collapse with decreased volume. In a trend comparable to the GGA calculations, these changes are accompanied by changes in the crystal structure features: illustrated by the intra- and interchain Cr−Cl distances, it can be seen that under low (and negative) pressure, the $CrCl_2$ chains remain basically intact, with variable interchain distance. Under high pressure, however, the $CrCl_2$ chains are pushed close to each other, with the ligand environment of the Cr atoms changing from a prolate to an oblate octahedron.

The electronic DOS, obtained from GGA + U calculations for the relaxed ground state and under high pressure, is shown in Figure 9. Similarly to the GGA result, a gap in the 3d bands

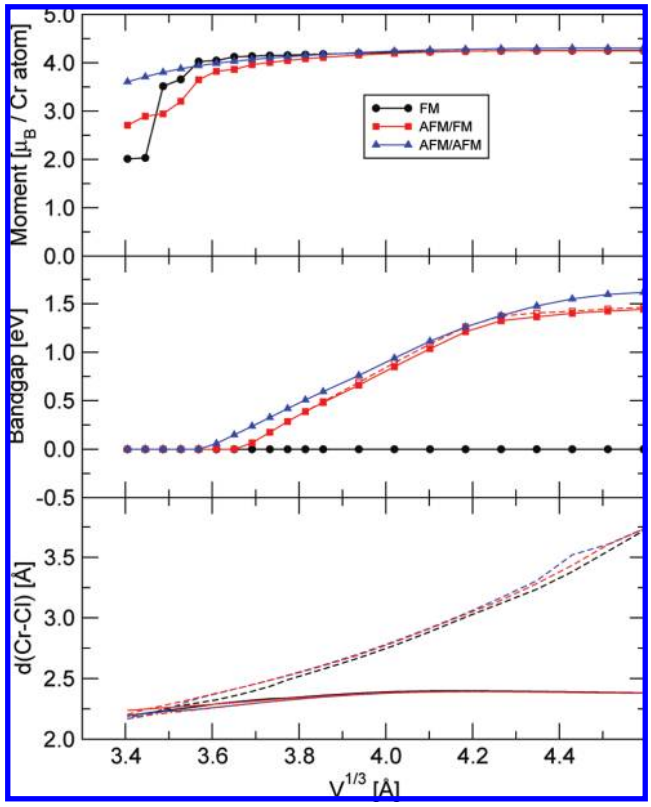

Figure 8. From top: magnetic moments, band gaps, and internal Cr−Cl bond lengths, depending on lattice constant, and for various magnetic coupling schemes, from GGA + U calculations. Bond lengths: solid (dashed) lines for intra- (inter-) chain distances.

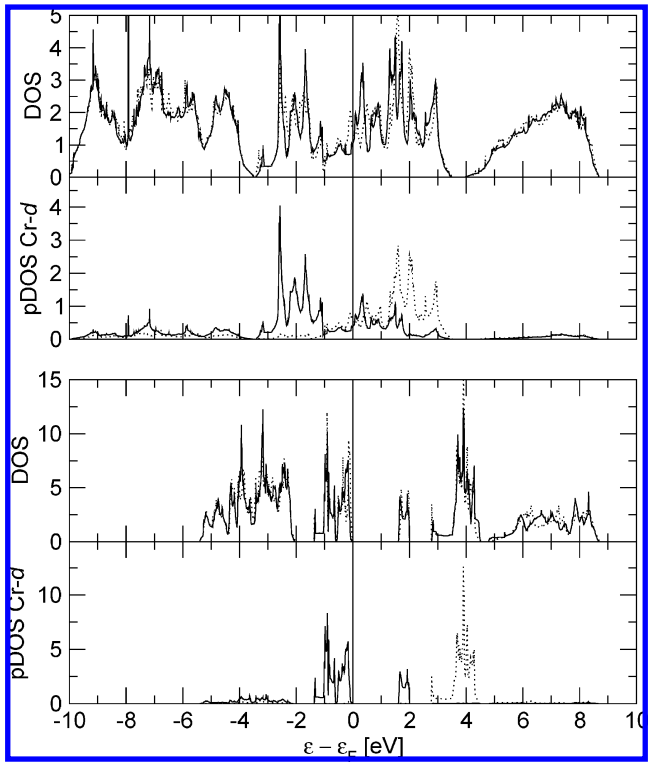

Figure 9. Electronic DOS of AFM/FM structure, from GGA + U calculations. Upper panel: $p \approx 500$ kBar; lower panel: $p = 0$. For details, see caption of Figure 5.

exists in the relaxed ground state. The energy difference between the two spin components is about 2 eV higher than in GGA, corresponding to the penalty term of 1.8 eV added to the total

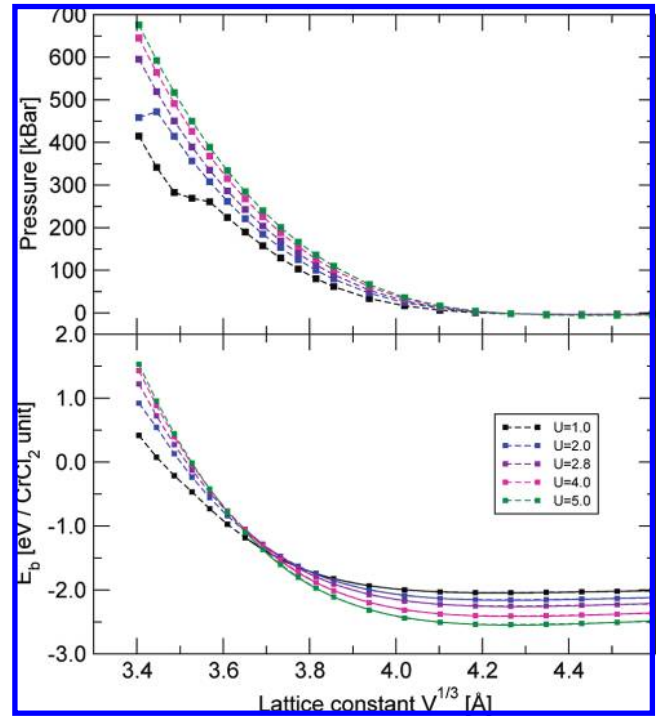

Figure 10. Total energies (lower panel) and pressures (upper panel) from GGA + U calculations for variable U.

energy expression. The bandwidth of the occupied 3d states is only about 1.5 eV, and they are separated from the Cl 2p electrons, which are about −2 ••• −5 eV below the Fermi level. Under pressure, however, and again similar to the GGA results, the energy difference and difference in occupation between the two spin components is lifted, and $CrCl_2$ becomes metallic.

The crystalline properties of $CrCl_2$ depend on the choice of the parameters U and J in the on-site interaction term. Table 1 lists ground state properties for a variety of values for U (with fixed $J = 1.0$ eV) around the otherwise preferred value of $U = 2.8$ eV. Increasing the U parameter from $U = 1.0$ eV (the GGA limit) to $U = 5.0$ eV leads to an increased binding energy and a decreased equilibrium unit cell volume but almost unchanged internal Wyckoff positions x and y. The intrachain (interchain) Cr−Cr distances increase (decrease) with increasing U. Overall, however, these changes are (with the exception of the binding energy) rather minute. The corresponding $E(V)$ and $p(V)$ curves are shown in Figure 10. They share the flat potential energy surface close to the global minimum that is usual for $CrCl_2$ but show significantly different behavior under pressure. Increasing U increases monotonically the pressure at any given unit cell volume. Thus, fitting the GGA + U method to experimental data at zero pressure might not be sufficient to study effects of high pressure on the respective system. In the present case, however, where no experimental pressure studies are available, the best possible approach is to adjust the GGA + U parameters to the ground state magnetic properties.

$CrCl_2$ in the ground state can be seen as a $S = 2$ Heisenberg antiferromagnet. Couplings between adjacent spin centers distinguish between intrachain coupling (via coupling constant J), and interchain coupling (via J'). Each spin center is coupled to two nearest intrachain and four nearest interchain neighbors. The coupling constants J and J' are calculated as outlined in ref 23 from energy differences of specific magnetic states. In the ground state, the GGA results of $J = -19.9k_B/K$ and $J' = 3.08k_B/K$ are much larger than estimated by experiment ($J = -9.5k_B/K$, $J' = 1.23k_B/K$);[24] the GGA + U results of $J =$

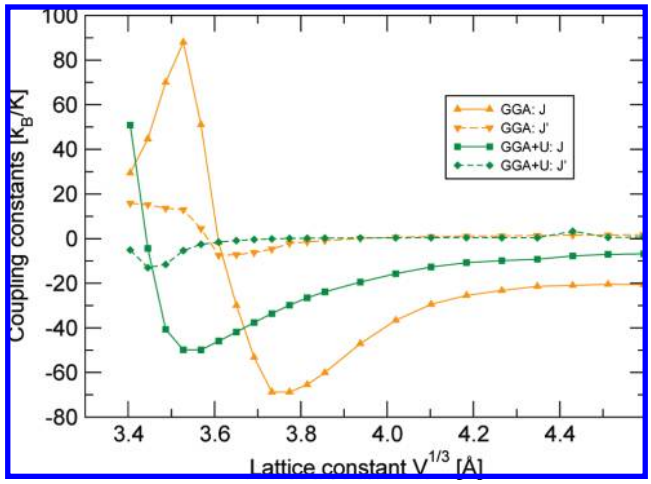

Figure 11. Magnetic coupling constants J, J' from GGA and GGA + U calculations.

$-9.6k_B/K$ and $J' = 1.46k_b/K$ are, however, close to experiment, with the value of $U = 2.8$ eV chosen to optimize this agreement. The volume dependence of the magnetic coupling constants is plotted in Figure 11. Both GGA and GGA + U show the same qualitative trend under pressure: the antiferromagnetic character of the intrachain coupling J is increased, up to a maximum of about $70k_B/K$ ($50k_b/K$) for GGA (GGA + U), about three times (five times) larger than at the relaxed ground state. Upon further compression (which corresponds to the transition to the metallic phase), the coupling constant J changes its sign, thus favoring ferromagnetic intrachain coupling. The antiferromagnetic interchain coupling J' becomes largest where J changes its sign, but is generally much weaker than the intrachain coupling.

Conclusions

In conclusion, we have presented first principles calculations on ground state properties of α-$CrCl_2$ under pressure. Both standard GGA and GGA + U calculations predict a metallic phase transition of $CrCl_2$ at a transition pressure of about 15 GPa (from GGA) and 35 GPa (from GGA + U), respectively. Both methods relate the change in the electronic structure to distinct changes in the crystalline and magnetic properties: the octahedral ligand environment of the Cr atoms changes from prolate to oblate, and the local magnetic moments collapse. Simultaneously, the magnetic coupling constants reach their maximal values and change drastically in magnitude and sign upon further compression of the crystal. It is, however, advisible to adjust the parameters U and J properly; that is, if possible, to available high pressure data. In the present study, material properties near the relaxed ground state show only a weak dependence on the choice of $U - J$; however, high pressure properties vary much stronger. Experiments are needed to verify the results obtained in our calculations.

Acknowledgment. We thank the Royal Society of New Zealand (Marsden grant 07-MAU-016) and EducationNZ for financial support.

References and Notes

(1) Badding, J. V. *Annu. Rev. Mater. Sci.* **1998**, *28*, 631.
(2) Grochala, W.; Hoffmann, R.; Feng, J.; Ashcroft, N. W. *Angew. Chem., Int. Ed.* **2007**, *46*, 3620.
(3) Tamblyn, I.; Raty, J.-Y.; Bonev, S. A. *Phys. Rev. Lett.* **2008**, *101*, 075703.
(4) Eremets, M. I.; Trojan, I. A.; Medvedev, S. A.; Tse, J. S.; Yao, Y. *Science* **2008**, *319*, 1506.
(5) Lundegaard, L. F.; Weck, G.; McMahon, M. I.; Desgreniers, S.; Loubeyre, P. *Nature* **2006**, *443*, 201.
(6) Gao, L.; Xue, Y. Y.; Chen, F.; Xong, Q.; Meng, R. L.; Ramirez, D.; Chu, C. W.; Eggert, J. H.; Mao, H. K. *Phys. Rev. B* **1994**, *50*, 4260.
(7) Tse, J. S.; Yao, Y.; Tanaka, K. *Phys. Rev. Lett.* **2007**, *98*, 117004.
(8) Schilling, J. S. *J. Phys. Chem. Solids* **1998**, *59*, 553.
(9) Mediavilla, C.; Tortajada, J.; Baonza, V. G. *J. Comput. Chem.* **2009**, *30*, 415.
(10) Gaston, N.; Paulus, B.; Rościszewski, K.; Schwerdtfeger, P.; Stoll, H. *Phys. Rev. B* **2006**, *74*, 094102.
(11) Paulus, B. *Phys. Rep.* **2006**, *428*, 1.
(12) Stoll, H. *J. Phys. Chem. A* **2009**, in press.
(13) Stoll, H.; Paulus, B.; Fulde, P. *Chem. Phys. Lett.* **2009**, *90*, 469.
(14) Ortmann, F.; Bechstedt, F.; Schmidt, W. G. *Phys. Rev. B* **2006**, *73*, 205101.
(15) Conroy, M. W.; Oleynik, I. I.; Zybin, S. V.; White, C. T. *J. Phys. Chem. A* **2009**, *113*, 3610.
(16) Cococcioni, M.; de Gironcoli, S. *Phys. Rev. B* **2005**, *71*, 035105.
(17) Anisimov, V. I.; Zaanen, J.; Andersen, O. K. *Phys. Rev. B* **1991**, *44*, 943.
(18) Kasinathan, D.; Kuneš, J.; Koepernik, K.; Diaconu, C. V.; Martin, R. L.; Prodan, I. D.; Scuseria, G. E.; Spaldin, N.; Petit, L.; Schulthess, T. C.; Pickett, W. E. *Phys. Rev. B* **2006**, *74*, 195110.
(19) Rollmann, G.; Rohrbach, A.; Entel, P.; Hafner, J. *Phys. Rev. B* **2004**, *69*, 165107.
(20) Zhang, W.-B.; Deng, Y.-H.; Hu, Y.-L.; Han, K.-L.; Tang, B.-Y. *Solid State Commun.* **2007**, *142*, 6.
(21) Bouchet, J.; Silberchicot, B.; Jollet, F.; Pasturel, A. *J. Phys.: Condens. Matter* **2000**, *12*, 1723.
(22) Janesko, B. G.; Henderson, T. M.; Scuseria, G. E. *Phys. Chem. Chem. Phys.* **2009**, *11*, 443.
(23) Hermann, A.; Vest, B.; Schwerdtfeger, P. *Phys. Rev. B* **2006**, *74*, 224402.
(24) Winkelmann, M.; Baehr, M.; Reehuis, M.; Steiner, M.; Hagiwara, M.; Katsumata, K. *J. Phys. Chem. Solids* **1997**, *58*, 481.
(25) Vest, B.; Varga, Z.; Hargittai, M.; Hermann, A.; Schwerdtfeger, P. *Chem.—Eur. J.* **2008**, *14*, 5130.
(26) Smith, S.; Hillier, I. H. *J. Chem. Soc., Chem. Commun.* **1989**, 539.
(27) Jacox, M. E.; Milligan, D. E. *J. Chem. Phys.* **1969**, *51*, 4143.
(28) Ogden, J. S.; Wyatt, R. S. *Dalton Trans.* **1987**, 859.
(29) Jensen, V. R. *Mol. Phys.* **1997**, *91*, 131.
(30) Bridgeman, A. J.; Bridgeman, C. H. *Chem. Phys. Lett.* **1997**, *272*, 173.
(31) Garner, C. D.; Hillier, I. H.; Wood, C. *Inorg. Chem.* **1978**, *17*, 168.
(32) Wang, S. G.; Schwarz, W. H. E. *J. Chem. Phys.* **1998**, *109*, 7252.
(33) Vest, B.; Schwerdtfeger, P.; Kolonits, M.; Hargittai, M. *Chem. Phys. Lett.* **2009**, *468*, 143.
(34) Kresse, G.; Furthmüller, J. *Phys. Rev. B* **1996**, *54*, 11169.
(35) Perdew, J. P.; Chevary, J. A.; Vosko, S. H.; Jackson, K. A.; Pederson, M. R.; Singh, D. J.; Fiolhais, C. *Phys. Rev. B* **1992**, *46*, 6671.
(36) Dudarev, S. L.; Botton, G. A.; Savrasov, S. Y.; Humphreys, C. J.; Sutton, A. P. *Phys. Rev. B* **1998**, *57*, 1505.
(37) Bengone, O.; Alouani, M.; Blöchl, P.; Hugel, J. *Phys. Rev. B* **2000**, *62*, 16392.
(38) Rohrbach, A.; Hafner, J.; Kresse, G. *J. Phys.: Condens. Matter* **2003**, *15*, 979.
(39) Blöchl, P. E. *Phys. Rev. B* **1994**, *50*, 17953.
(40) Kresse, G.; Joubert, D. *Phys. Rev. B* **1999**, *59*, 1758.
(41) Vinet, P.; Ferrante, J.; Smith, J. R.; Rose, J. H. *J. Phys. C: Solid State Phys.* **1986**, *19*, L467.
(42) Tracy, J. W.; Gregory, N. W.; Lingafelter, E. C.; Dunitz, J. D.; Mez, H.-C.; Rundle, R. E.; Scheringer, C.; Yakel, H. L., Jr.; Wilkinson, M. K. *Acta Crystallogr.* **1961**, *14*, 927.
(43) Perdew, J. P.; Parr, R. G.; Levy, M.; Balduz, J. L. *Phys. Rev. Lett.* **1982**, *49*, 1691.

JP904325V